Melting behaviour investigation of municipal solid waste incineration fly ash samples from different incineration technologies for metal recovery: An integrated experimental and thermodynamic modelling approach

E. Soylu[1] and *G.Tranell*[2]

1.PhD-candidate, Norwegian University of Science and Technology, 7004. Email: ece.soylu@ntnu.no
2.Prof, Norwegian University of Science and Technology, 7004. Email: gabriella.tranell@ntnu.no

ABSTRACT

Municipal solid waste incineration fly ash (MSWI FA) is an important waste product that holds considerable potential for valorisation. In addition to major phases such as $CaSO_4$, $CaCO_3$, $NaCl$, KCl, and silicates, these ashes contain significant amounts of valuable elements like copper (Cu), zinc (Zn), lead (Pb), and others, where the specific composition depends on the source of the waste and the incineration process used. This study aims to investigate the melting behaviour of municipal MSWI FA samples from various incineration technologies, including rotary kiln, grate furnace, and circular fluidized bed, as a background for pyro/hydrometallurgical metal extraction. The experimental study was designed to research the effect of salt composition on the melting temperature and phase formations of different ash types, as well as metal migration between phases, using a sessile drop furnace. As a complimentary approach to the experimental study, thermodynamic modelling (FACTSage© 8.3) was used to predict the phase formations of different fly ashes using Scheil-Gulliver cooling of molten ash. The observed melting point of the samples varied between 1000 °C – 1400 °C depending on the ash type, without any trend of salt composition effect on the melting point. Upon solidification, there were three distinct phases observed in the samples: a metallic phase, a crystalline, non-metallic phase with inhomogeneous shape pattern, and an amorphous matrix phase. The findings indicate that the predominant component in the matrix phase was Ca-O-Si, implying the formation of calcium silicate slag. Elemental mapping showed metallic droplets consisting of primarily Fe-P phases, while the crystalline non-metallic phase is concentrated in Ca and S. The furnace atmosphere (Ar vs CO) had no significant impact on the phase formations. Thermodynamic modelling results were in good agreement with the experimental study, except for P-rich metallic phases, showing the formation of non-metallic and complex silicate slag phase formations.

INTRODUCTION

Municipal solid waste incineration fly ash (MSWI FA) is a by-product of the incineration process, which involves the combustion of waste at high temperatures reducing its volume by 85-90%, mass by 60-90%, and organic matter by up to 100% (Zhang et al., 2021). Globally, the share of incineration in waste management practices is 11%, where bottom ash and fly ash residue from MSWI account for approximately 30wt% and 1-5wt% of the input waste weight, respectively (Kaza et al. 2018; Tian et al. 2021). Different technologies such as grate, rotary kiln, and fluidised bed are used for incineration practices. In Europe, approx. 90 % of MSW treatment installations are grates, where the share of fluidised beds and rotary kiln are 5% and 2%, respectively (Neuwahl et al. 2019). The operation temperature of incinerators varies depending on the feed material and incineration plant, which results in high versatility in the ash composition (Nedkvitne et al., 2021). FA contains considerable number of high-value metals such as Zn, Cu, Ni, Co, etc. along with silicates and varying calcium bearing compounds with a potential of being used in different industries such as construction and glass ceramics (Zhao et al. 2021; Fan et al. 2022). A study where the chemical composition of approximately 900 different FA samples were analysed showed that 1 kg of fly ash

contains 10 grams of Zn and 1.2 grams of Cu, on average (Nedkvitne et al. 2021). Even though the variations are high, and composition of FA depends on many factors such as location, season, incineration technology used, etc., FA holds a great potential for recovery of critical metals competing with the ore grades in the concentration of critical metals (Nedkvitne et al. 2021; Nedkvitne et al. 2023). The current best available technologies (BATs) for utilization of FA are: 1) stabilization of heavy metals in FA, 2) utilization of FA as construction material after stabilization, and 3) resource recovery in the means of metal and salt extraction via thermal/hydrometallurgical processes. (Jadhav and Hucheng 2012; Michaël Becidan 2018; Wang et al. 2021).

There are various studies on the melting characteristics of FA. One study investigated the effect of the chemical composition on metal separation efficiency during melting (Okada and Omikawa 2013). It was observed that decreasing the Cl to Na and K molar ratio in the ash reduced Fe and Cu volatilization, enhancing metal separation. The studies that investigated the impact of atmosphere on the volatility of metals revealed that volatility of metals was also affected by the amount of liquid slag formed and the temperature. It was concluded that under oxidizing conditions and elevated temperatures, elements like As, Bi, Sb, Sn, and Zn tended to be mainly concentrated in condensed phases, whereas, under reducing conditions and high temperatures, these elements were predominantly released into the gas phase, however, Cu and Pb volatility was suppressed under reducing conditions (Lane et al. 2020a; Lane et al. 2020b). Another study suggested a reverse trend for Zn, reducing atmosphere hindering vaporization of Pb, Zn, Cu, Cr, Co, and Ni due to increased liquid slag formation (Jiao et al. 2022). Other study that investigated the melting characteristic of FA concluded that ash composition was the main parameter affected the melting temperature, whereas atmosphere had minimal impact by a slight shift to higher temperature in oxidizing atmosphere. Also, addition of CaO increased the melting point by the formation of new compounds (Li et al., 2007). In one study, it was found that all crystalline structures transformed into molten slag at temperatures exceeding 1300 °C (Gao et al., 2021).

Metal extraction from FA via hydrometallurgical methods, has been extensively investigated in the literature (Karlfeldt Fedje et al. 2010; K. Huang et al. 2011; Tang & Steenari 2016; Jadhav & Hocheng, 2012; Wen et al. 2020; Wang et al. 2021). In terms of metal extraction via pyrometallurgical processes, the main approach has been thermal separation of heavy metal (HM) compounds by taking the advantage of the high volatility of chlorides (Nowak et al. 2012; Yu et al. 2016; Wang et al. 2021). Experimental findings indicated that both Pb and Zn possess considerable volatility, with approximately 80% volatilization achieved at 900°C even without the addition of chlorination agents (Kurashima et al. 2019). Another pyrometallurgical method investigated for metal extraction from FA is molten salt treatment, in which molten salt served as a metal extraction and separation medium, and requiring relatively low-temperature (600-800 °C) processes (Xie et al. 2020). Commonly used reagents include chloride-based salts such as sodium chloride (NaCl) and potassium chloride (KCl), as well as eutectic salt mixtures (e.g. $NaCl\text{-}CaCl_2$).

Even though there are considerable number of technologies available for ash valorisation, the complexity, compositional variations, and relatively low metal concentrations are the biggest limitations for techno-economically robust solutions. This study aims at giving insights into the melting behaviour of different ash types with the prospect of utilising thermal treatment for metal recovery as a part of more holistic FA recovery process. The main focus of the study was on investigating the metallic, non-metallic, and amorphous phase formations upon melting as a basis for potential exploitation of leachability of different crystal structures in varying mediums.

MATERIALS AND METHODS

The fly ash samples investigated in this study were obtained from different incineration plants located in various countries and using different incineration technologies, such as grate furnace (denoted as GF), rotary kiln (denoted as R), and circular fluidized bed (denoted as C). Both raw and salt-washed fly ash samples are used for the experiments, with 'W' denoting the washed samples. The samples were melted without any prior compacting or pelletizing steps. The particle size of the raw and washed samples ranges between 37.66-139.52 μm and 30.41-83.38 μm, respectively. The chemical composition of the samples is presented in Table 1. It was determined via X-ray diffraction that the major compounds in fly ash samples were salts (such as KCl, NaCl, and $NaSO_4$), Ca-compounds (including CaO, $CaCO_3$, and $CaSO_4$), and complex alumina silicates.

Table 1. ICP-MS results of ash samples. (Reduced table containing only major and critical elements).

Elements	wt. %									
	R	GF1	GF2	GF3	C	RW	GF1W	GF2W	GF3W	CW
Al	1.80	2.10	2.10	3.60	1.20	3.50	7.70	4.20	4.70	10.00
Ba	1.60	0.11	0.07	0.28	0.19	3.30	0.13	0.10	0.33	0.21
Ca	3.30	30.00	28.00	21.00	23.00	6.60	23.00	29.00	24.00	22.00
Cl	8.00	9.90	12.00	3.80	3.80	0.36	0.31	0.36	0.15	0.38
Cu	0.27	0.06	0.05	0.08	0.47	0.49	0.07	0.09	0.08	0.57
Fe	2.80	1.20	0.92	2.10	1.90	6.00	2.40	1.80	2.50	2.60
K	5.20	2.20	2.10	4.30	0.91	2.50	0.56	0.34	0.66	0.45
Mg	0.58	0.78	0.70	0.15	1.50	1.20	1.50	1.50	2.00	2.00
Mn	0.15	0.05	0.05	0.10	0.10	0.30	0.08	0.11	0.16	0.13
Mo	0.10	0.00	0.00	0.00	0.02	0.19	0.00	0.00	0.00	0.00
Na	19.00	2.70	3.40	5.20	1.90	7.20	0.64	0.58	0.79	0.93
Ni	0.10	0.00	0.01	0.01	0.01	0.21	0.01	0.02	0.01	0.02
P	5.90	0.55	0.44	0.75	0.35	11.00	0.71	0.78	0.88	0.47
Pb	0.35	0.21	0.18	0.31	0.20	0.44	0.12	0.20	0.20	0.21
S	8.40	3.60	4.50	11.00	1.60	1.00	2.40	4.00	8.00	1.80
Si	3.60	5.70	3.70	6.60	9.30	6.60	11.00	7.50	8.40	12.00
Ti	1.10	0.54	0.49	1.30	0.24	2.20	1.00	1.00	1.60	1.70
Zn	2.30	0.82	0.82	1.90	0.45	4.50	1.30	1.50	2.30	0.60

In the experimental setup, a sessile drop furnace was employed to investigate the melting behaviour of fly ash samples. The furnace is composed of a stainless-steel chamber with two windows, featuring a graphite heating element and radiation shield, a pyrometer, and a control C-type thermocouple. Additionally, the furnace is equipped with a high-speed digital CCD camera (Microtron MC 1310, Microtron GmbH, Unterschleissheim, Germany) at 50 frames per second, allowing real-time observation of the samples during heating (Bao et al. 2021; Bublik et al. 2021; Canaguier and Tangstad 2021). To determine the melting point, the ash samples were heated under argon (Ar, 99.9999 pct purity) atmosphere until the onset of melting was observed in the camera. Before starting the experiments, a calibration experiment with pure iron (Fe) was done to ensure accurate temperature reading. To investigate the salt composition effect on melting temperature, one set of ash samples was washed with water to remove salts and one set of samples are used without any treatment. Based on the melting temperature observations in these experiments, a second part of experiments was conducted at T_m+100 °C with a holding time of 1 hour, and under both Ar and carbon monoxide (CO, 99.9993 pct purity) gas atmospheres. Only washed samples were used in the subsequent experiments. The focus of the second set of experiments was to observe the phase disintegrations and metal migration after melting, and to investigate the effect of a reducing atmosphere (when CO is used) on the system. All experiments were conducted with a consistent gas flow of 0.1 L/min. Alumina was used as the substrate for the experiments, and the sample amount varied between 80-100 mg. The characterization of ash melts was done using Scanning Electron Microscopy-Energy Dispersive Spectroscopy (SEM-EDS) and Electron Probe Micro-Analysis (EPMA), and samples were epoxy-cast twice to get cross-sectional imaging.

The thermodynamic modelling study was conducted using FACTSage© 8.3 software (Thermfact/CRCT, Montreal; GTT-Technologies, Aachen), where the Gibbs free energy minimization is applied. The phase formation upon solidification was modelled in the Equilibrium module selecting FactPS and FTOxide databases (FACTSage 8.3 - Summary of databases, no date). To simplify the system, the chemical composition of ash samples was registered as the main sulphate or carbonate compounds, depending on the sample composition, where the quantitative data was obtained by Rietveld analysis of XRD scanning, and for metal oxides deriving from elemental composition data provided in Table 1.

RESULTS AND DISCUSSION

Effect of salt composition on the melting temperature

The melting temperatures of the raw and salt washed MSWI fly ash samples were determined based on the visual observations with a high-speed digital camera during heating. The images are shown in Figure 1, where the first clear images were taken when the temperature reached 900 °C. A complete wetting at the melting point was observed for all samples, except sample R. During the heating of sample GF3, gasification of some amount of sample was recorded when the temperature reached close to the melting point, and the evaporation accelerated with further increase in the temperature. On the other hand, sample GF3W did not show any excess gasification, however, bubbling on the melt surface was observable to some extent. This suggests the evaporation of chlorine compounds in the unwashed samples, whereas the removal of most chlorine salts after washing limits the gasification in the washed sample. The results show that the melting temperature of the fly ash samples varies between 1000 °C – 1400 °C, depending on the ash type and the effect of decreased salt content (Table 2). Salt washing did not have the same effect for all ash types, the melting temperature of samples R and C decreases, whereas the melting point of samples GF1 and GF3 remains constant after salt removal. An increase in melting temperature was observed only in sample GF2. These results were higher than the reported melting temperatures of FA in the literature. According to the previous search results, the melting temperature of MSWI fly ash varied depending on the specific conditions and composition of the sample. One study found that the melting process of fly ash consisted of three main transitions: dehydration (100-200 °C), polymorphic transition (480-670 °C), and fusion (1101-1244 °C) (Li et al. 2007). Another study reported that the ash fusion temperatures of MSWI fly ash ranged from 1167 °C to 1211 °C (Gao et al., 2021).
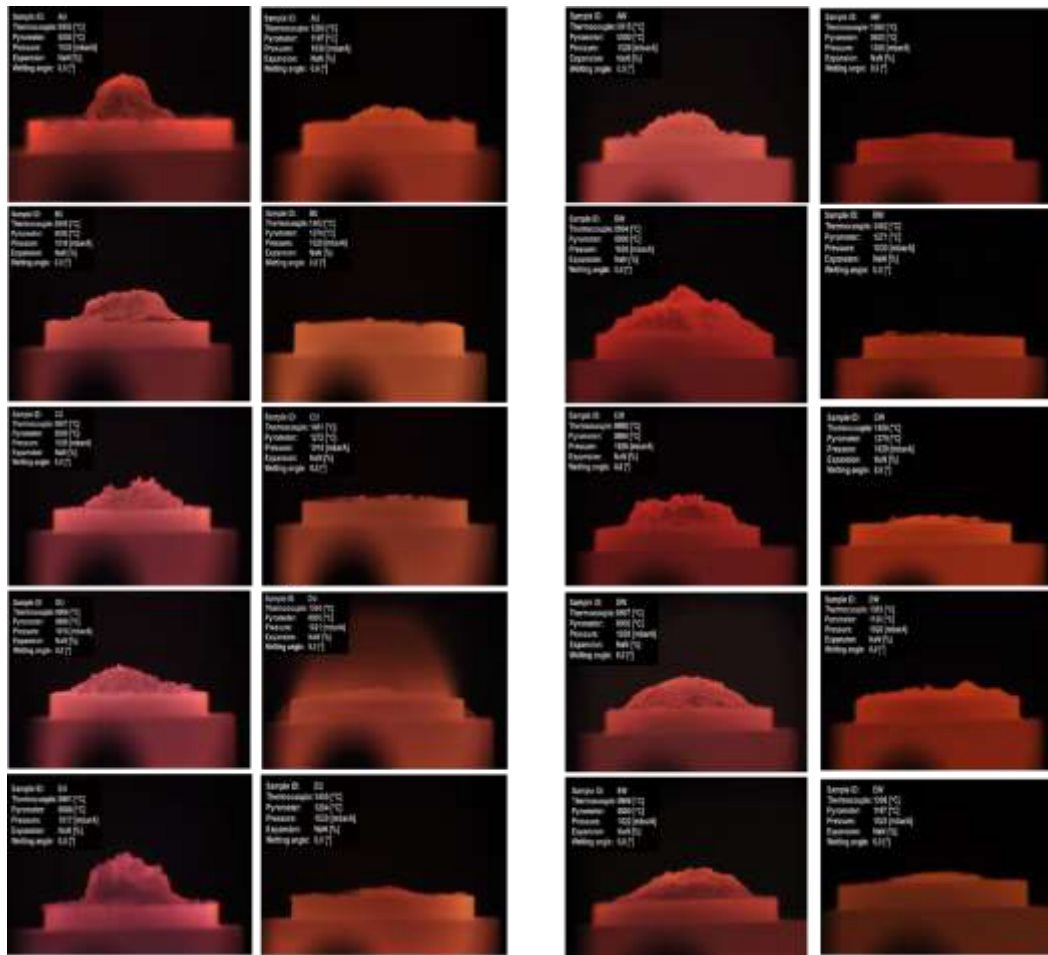
Figure 1. Images captured during the heating of fly ash samples (Registered sample IDs in the furnace and their corresponding sample denotations: AU=R, AW=RW, BU=GF1, BW=GF1W, CU=GF2, CW=GF2W, DU=GF3, DW=GF3W, EU=C, and EW=CW).

Table 2. Approximate melting temperatures of raw and washed ash samples.

SAMPLE	Tm (°C)	SAMPLE	Tm (°C)
R	1200	RW	1000
GF1	1400	GF1W	1400
GF2	1200	GF2W	1400
GF3	1300	GF3W	1300
C	1400	CW	1300

Effect of chemical composition and atmosphere on phase formations and metal migration

To investigate the effect of composition on solidification, three representative samples were chosen based on their major compounds: RW (Na_2SO_4-rich), GF1W ($CaCO_3$-rich), and GF3W ($CaSO_4$-rich). The SEM-EDS results of the melted and solidified ash samples under Ar and CO atmospheres are shown in Figure 2 and Figure 3, respectively. The results suggest that there are three distinct phases upon solidification: a metallic phase, a crystalline, non-metallic phase with inhomogeneous shape pattern, and an amorphous matrix phase. The EDS data points show that metallic droplets mainly contain Fe and phosphorous (P), with some extent of silicon (Si), and other elements such as molybdenum (Mo), nickel (Ni), aluminium (Al), titanium (Ti) and manganese (Mn) found in the metallic phase depending on the initial sample composition. In some samples (Figure 2b and Figure 3a), Cu is found in Fe-containing metallic phases, suggesting coalescence upon reduction. In Figure

5

2b, the Cu concentration is high (67.54%) with no P detected in the phase. EDS data points of non-metallic phases reveals that the phase is mainly composed of calcium (Ca) and sulfur (S), suggesting the formation of a CaS phase. It is also observed that non-metallic phases contain some amount of Si, O, Mn, and Al (Figure 2c and Figure 3a-c), suggesting migration of these elements into the CaS phase. The formation of CaS can be attributed to the reduction of $CaSO_4$ during melting, which also suggests that some extent of reductive conditions provided in the system also under Ar atmosphere that led to formation of CaS, eg in sample GF3W. The sources of reductant, possibly carbon (C), can be the graphite furnace wall in the sessile drop furnace and the elemental C present in the initial composition of the ash. The analysis of carbon is not available for the samples used in this study; however, it is known that most ash samples might contain significant amount of C (5-20 wt.%) coming from flue gas cleaning operations where activated carbon is added (Geng et al. 2020). In sample RW, S is not found in the Ca-rich non-metallic phase, as opposed to the detected amount of O which is high along with some amount of P, suggesting the formation of $Ca_5(PO_4)$ phase. The results suggest the formation of amorphous Ca-rich $CaO-SiO_2-Al_2O_3$ slag phase as the matrix in the samples where $CaCO_3$ and $CaSO_4$ are the major compounds. In sample RW, however, Ca is not detected in the matrix phase and the results suggest that it is composed of complex $SiO_2-Al_2O_3-K_2O-P_2O5-Na_2O$ slag. In terms of the effect of atmosphere on phase formations, there is no substantial difference between phases that could be linked to furnace atmosphere.
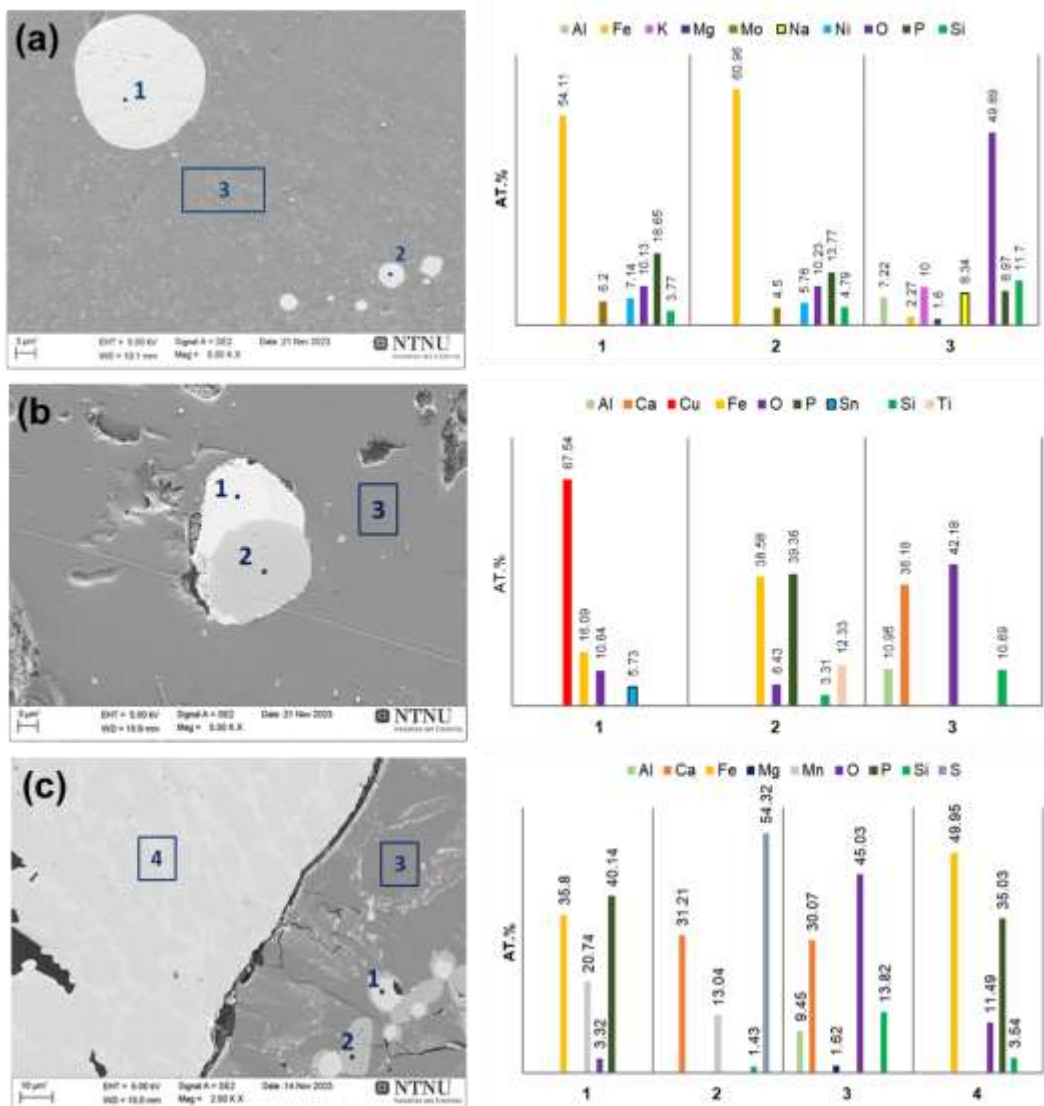
Figure 2. SEM-EDS results of ash melts under AR atmosphere: a) RW, b) GF1W, and c) GF3W.

6
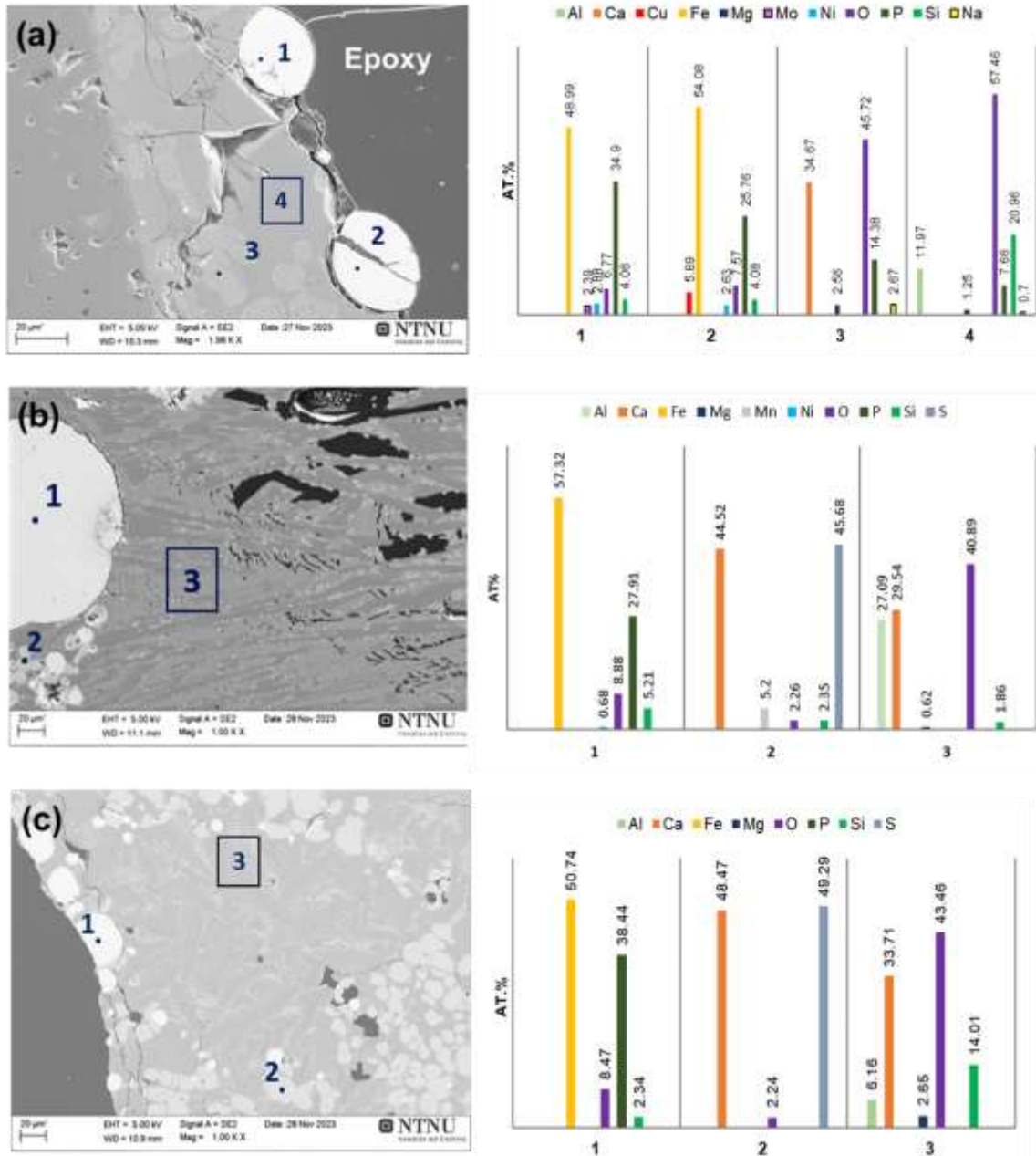
Figure 3. SEM-EDS results of ash melts under CO atmosphere: a) RW, b) GF1W, and c) GF3W.

Elemental mapping in EPMA correlates well with the EDS data, except for O, where EPMA imaging does not show any O in the Fe-P phase regions as opposed to EDS spectra (Figure 4), as would be expected. It is also observed that metallic droplets composed of two phases, suggesting solidification into different Fe-rich phases, eg Fe_3P and Fe_2P, upon solidification (Okamoto 1990). The images showed some amount of Cu and Zn in the metallic phase, which indicates reduction followed by coalescence. Differently from EDS results, Zn and Cu are found throughout the sample, concentrating in the metallic phase. The elemental map confirms the formation of non-metallic CaS and Ca-P phases having some amount of Na along with O. The oxygen concentration in the Ca-phase (Figure 4a) is less than P and Ca, which differs from EDS data. Figure 4b suggests regions in the matrix phase where Al_2O_3 and SiO_2 concentrated.
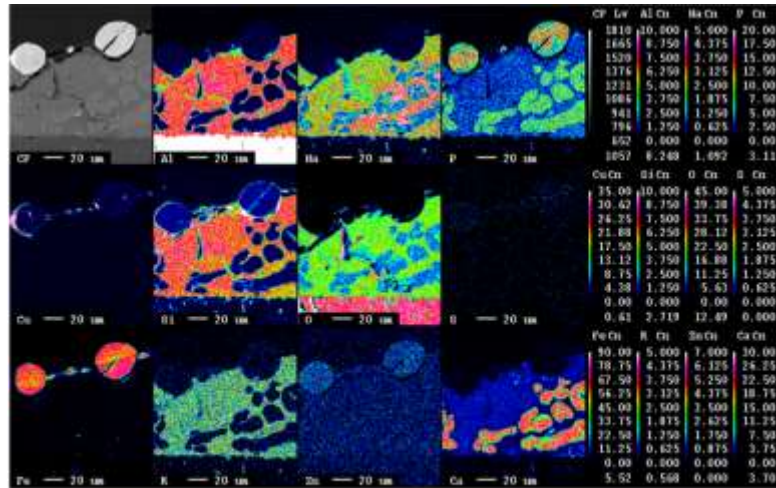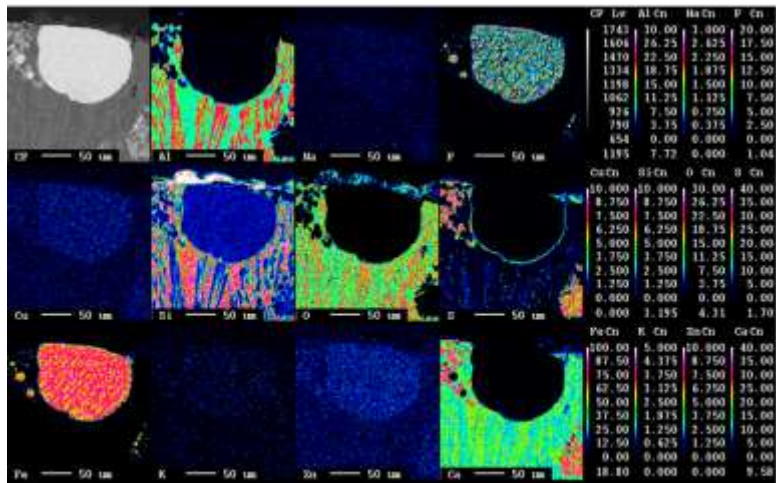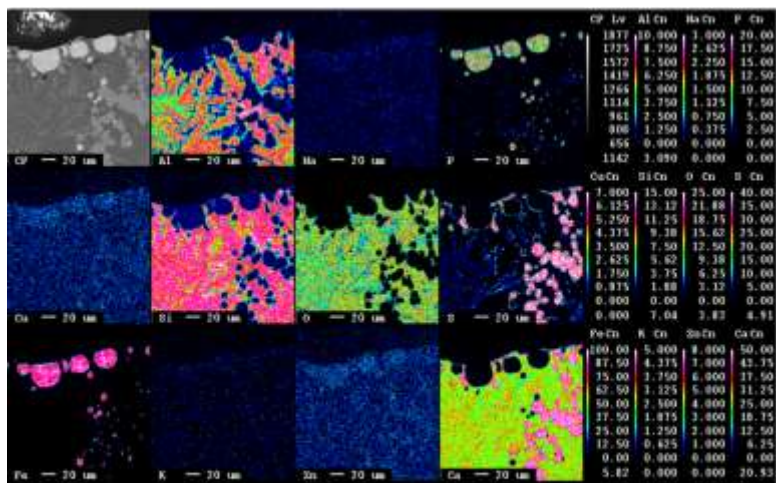
Figure 4. EPMA results of selected ash samples melted under CO: (a) RW, (b) GF1W, and (c) GF3W.

FACTSage© modelling

In Figure 5, the calculations of equilibrium phases during heating and cooling of the representative samples under CO atmosphere are shown. Taking into account the composition of the ash systems, initial compositions were used as input to the calculations as shown in Table 4. The melting temperature is interpreted as the temperature where liquid slag formation starts in the heating graphs. The calculated melting temperature of RW and GFW1 is 700 °C, and the melting temperature of GF3W is 1300 °C. The highest correlation between the calculations and the experimental observations is shown in GF3W, while calculated temperatures are lower than the experimental temperatures for the other samples. It is important to note that the melting temperature indicates complete melting of the samples in the experimental observations, whereas, thermodynamic modelling shows the melting initiation temperatures. In the experimental study, high-temperature recording is only possible after 900 °C, thus, melting initiation temperatures can not be observed for low temperatures. The registered complete melting temperatures correspond the temperatures where liquid slag formation has reached its peak, which corresponds to 1100 °C for RW, and 1400 °C for GF1W and GF3W. In terms of the effect of the dominant compounds on the melting temperatures, it is concluded that high concentration of Na_2SO_4 decreases the melting point, whereas high amounts of Ca-bearing compounds have the opposite effect. The phase formation upon solidification of different ash types was calculated by cooling the liquid slag from 1600 °C, using the Scheil-Gulliver functionality in FACTSage©. The temperatures for complete solidification were found as 537 °C, 642 °C, and 546 °C for RW, GF1W, and GF3W, respectively. The systems that include $CaSO_4$ shows CaS formation upon cooling, whereas, the calculations suggest the formation of $Na_2Ca_2P_2O_7$ and $Na_2CaP_2O_8$ compounds in RW. In regards to metallic phases, the thermodynamic calculations suggest the presence of FeS and ZnS compounds, starting to form later in the solidification stage. The modelling results on metallic phase formation does not correlate with the experimental observations, where results indicate the solidification of Fe-P compounds. This can be attributed to the well-known limitations in the FACTSage databases for P containing compounds. The modelling results show the formation of complex silicates ($K_2MgSi_3O_8$, $CaMgSi_2O_6$, $Ca_2FeSi_2O_7$, $Ca_2Al_2SiO_7$, $Ca_7P_2SiO_2O_{16}$, etc) showing a good correlation with the experimental matrix phase observations. The system that has $CaSO_4$ as the major compound shows silicate containing oxide solid solutions (FToxid-BRED, FToxid-bC2SA, and FToxid-Mel_A) along with $Ca_7P_2Si_2O_{16(s)}$ phase[1].

Table 3. Compositional data used for FACTSage© 8.3 calculations.

RW			GF1W			GF3W	
wt%			wt%			wt%	
Na_2SO_4	38.91		$CaCO_3$	55.06		$CaCO_3$	2.09
Al_2O_3	6.17		$CaSO_4$	9.23		$CaSO_4$	64.13
Fe_2O_3	8.00		Al_2O_3	11.13		Al_2O_3	7.49
MgO	1.86		Fe_2O_3	2.62		Fe_2O_3	3.01
MnO	0.18		MgO	1.90		MgO	2.80
SiO_2	13.18		SiO_2	18.00		SiO_2	15.15
P_2O_5	23.52		P_2O_5	1.24		P_2O_5	1.70
K_2O	2.81		K_2O	0.52		K_2O	0.67

---

[1] [FToxid-Bred] Bredigite OXIDE solution: $Ca_3(Ca,Mg)_4Mg(SiO_4)_4$ – a solid solution originating from $Ca_7Mg(SiO_4)_4$ by substitution of some Ca by Mg. [FToxid-bC2SA] OXIDE solution alpha-prime $(Ca,Sr,Ba)_2SiO_4$: Ca_2SiO_4 – Sr_2SiO_4 – Ba_2SiO_4 solution + (Mg_2SiO_4, Fe_2SiO_4, Mn_2SiO_4, Pb_2SiO_4, Zn_2SiO_4, $Ca_3B_2O_6$ in dilute amounts). End-members in pure compound database FToxidBase.cdb: $Ca_2SiO_4(S2)$, $Sr_2SiO_4(S2)$ and $Ba_2SiO_4(S1)$.

[FToxid-Mel_A] OXIDE solution-melilite: Mineralogical names: Akermanite ($Ca_2MgSi_2O_7$), Iron-akermanite ($Ca_2FeSi_2O_7$), Gehlenite ($Ca_2Al_2SiO_7$), Iron-gehlenite ($Ca_2Fe_2SiO_7$), Hardystonite ($Ca_2ZnSi_2O_7$). End-members in pure compound database FToxidBase.cdb: $Ca_2MgSi_2O_7$, $Ca_2FeSi_2O_7$, $Ca_2Al_2SiO_7$, $Ca_2ZnSi_2O_7$, $Pb_2ZnSi_2O_7$.

9
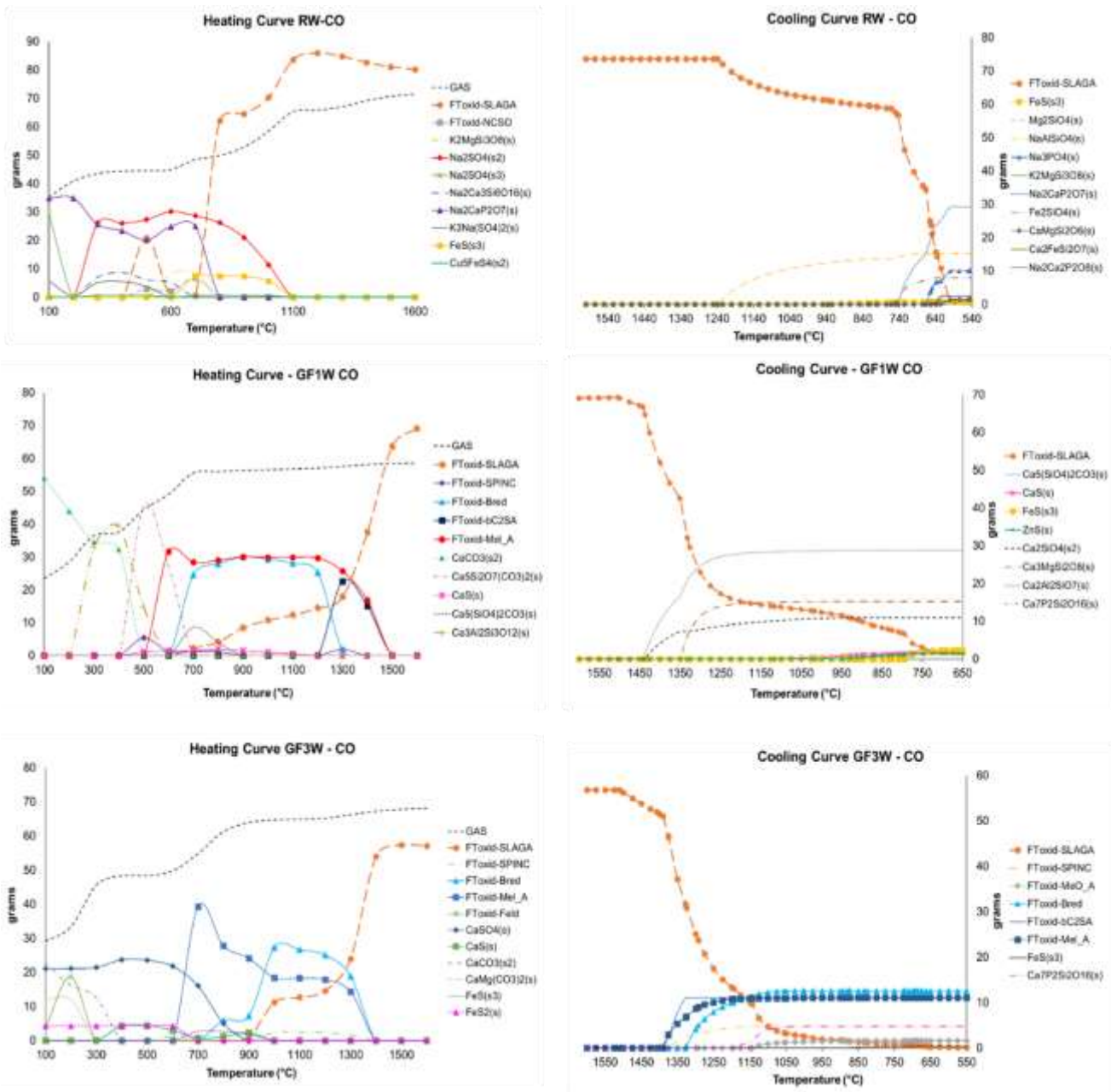
Figure 5. FACTSage© 8.3 calculations.

CONCLUSION

In conclusion, the findings of this study reveal that, not surprisingly, the most significant effect that has an impact on melting temperature and phase formation upon solidification is the composition of the ash samples. The experimentally observed melting points of the raw and salt-washed samples ranged from 1000 °C to 1400 °C, showing differences before and after salt-washing, however, without exhibiting a discernible trend. Both experimental findings and thermodynamic modelling indicate that an elevated concentration of Na_2SO_4 lowers the melting point, while the presence of Ca-bearing compounds has the opposite effect. The findings indicate that during the solidification process, three separate phases form: a metallic phase, a non-metallic phase with a crystalline structure and an uneven shape pattern, and a phase characterized by an amorphous matrix. The EDS data show that metallic droplets mainly contain Fe and P, whereas non-metallic phase is mainly composed of Ca-S, suggesting the formation of CaS under reducing conditions. In some samples, low concentration of other metals such as Cu, Ni, Mo, etc were detected in the metallic phase, indicating a co-reduction followed by coalescence mechanism. Also, in the CaS phase, the migration of some elements such as Si, O, Mn, and Al into the non-metallic phase is observed. The results indicate the formation of an amorphous Ca-rich CaO-SiO_2-Al_2O_3 slag phase as the predominant

10

matrix in samples characterized by the presence of $CaCO_3$ and $CaSO_4$ as major compounds. Conversely, in sample RW, the absence of Ca in the matrix phase suggests a composition comprising a complex SiO_2-Al_2O_3-K_2O-P_2O_5-Na_2O slag. Regarding the influence of atmospheric conditions on phase formation, no discernible distinctions were observed between phases that could be attributed to variations in the furnace atmosphere. The modelling results were in good correlation showing the formation of complex silicates ($K_2MgSi_3O_8$, $CaMgSi_2O_6$, $Ca_2FeSi_2O_7$, $Ca_2Al_2SiO_7$, $Ca_7P_2SiO_2O_{16}$, etc) as the major components in the solidified system.

REFERENCES

Bao, S. et al. 2021. Investigation of Two Immiscible Liquids Wetting at Elevated Temperature: Interaction Between Liquid FeMn Alloy and Liquid Slag. *Metallurgical and Materials Transactions B: Process Metallurgy and Materials Processing Science* 52(5), pp. 2847–2858.

Bublik, S., Bao, S., Tangstad, M. and Einarsrud, K.E. 2021. Interfacial Behaviour in Ferroalloys: The Influence of Sulfur in FeMn and SiMn Systems. *Metallurgical and Materials Transactions B: Process Metallurgy and Materials Processing Science* 52(6), pp. 3624–3645.

Canaguier, V. and Tangstad, M. 2021. In situ observation of the carbothermic reduction and foaming of slags in silicomanganese production. *Processes* 9(11).

FACTSage 8.3 – Summary of databases (no date). Available at: https://www.crct.polymtl.ca/fact/Documentation/FSData.htm

Fan, C., Wang, B., Ai, H. and Liu, Z. 2022. A comparative study on characteristics and leaching toxicity of fluidized bed and grate furnace MSWI fly ash. *Journal of Environmental Management* 305.

Gao, J., Wang, T., Zhao, J., Hu, X. and Dong, C. 2021a. An experimental study on the melting solidification of municipal solid waste incineration fly ash. *Sustainability (Switzerland)* 13(2), pp. 1–10.

Geng, C., Liu, J., Wu, S., Jia, Y., Du, B. and Yu, S. 2020. Novel method for comprehensive utilization of MSWI fly ash through co-reduction with red mud to prepare crude alloy and cleaned slag. *Journal of Hazardous Materials* 384.

Huang, K., Inoue, K., Harada, H., Kawakita, H., & Ohto, K. 2011. Leaching of heavy metals by citric acid from fly ash generated in municipal waste incineration plants. *Journal of Material Cycles and Waste Management*, *13*(2), 118–126. Jadhav, U.U. and Hocheng, H. 2012. A review of recovery of metals from industrial waste. *Journal of Achievements in Materials and Manufacturing Engineering* 54(2), pp. 154–167.

Jiao, F., Ma, X., Liu, T., Wu, C., Hanxu, L. and Dong, Z. 2022. Effect of Atmospheres on Transformation of Heavy Metals during Thermal Treatment of MSWI Fly Ash: By Thermodynamic Equilibrium Calculation. 2018. *Molecules* 27(2), pp. 738–754.

Kaza, S., Yao, L., Bhada-Tata, P. and Woerden, F. Van. *Urban Development Series: What a Waste 2.0.*

Karlfeldt Fedje, K., Ekberg, C., Skarnemark, G., & Steenari, B. M. 2010. Removal of hazardous metals from MSW fly ash-An evaluation of ash leaching methods. *Journal of Hazardous Materials*, *173*(1–3), 310–317.

Kurashima, K., Matsuda, K., Kumagai, S., Kameda, T., Saito, Y. and Yoshioka, T. 2019. A combined kinetic and thermodynamic approach for interpreting the complex interactions during chloride volatilization of heavy metals in municipal solid waste fly ash. *Waste Management* 87, pp. 204–217.

Lane, D.J. et al. 2020a. Thermal treatment of municipal solid waste incineration fly ash: Impact of gas atmosphere on the volatility of major, minor, and trace elements. *Waste Management* 114, pp. 1–16.

Lane, D.J., Hartikainen, A., Sippula, O., Lähde, A., Mesceriakovas, A., Peräniemi, S. and Jokiniemi, J. 2020b. Thermal separation of zinc and other valuable elements from municipal solid waste incineration fly ash. *Journal of Cleaner Production* 253.

Li, R., Wang, L., Yang, T. and Raninger, B. 2007. Investigation of MSWI fly ash melting characteristic by DSC-DTA. *Waste Management* 27(10), pp. 1383–1392.

Michaël Becidan. 2018. *Fly ash treatment technologies: An overview of commercial and upcoming technologies for Norway and Scandinavia*.

Nedkvitne, E.N., Borgan, Ø., Eriksen, D.Ø. and Rui, H. 2021. Variation in chemical composition of MSWI fly ash and dry scrubber residues. *Waste Management* 126, pp. 623–631.

Nedkvitne, E.N., Eriksen, D.Ø. and Omtvedt, J.P. 2023. Grade and Tonnage Comparison of Anthropogenic Raw Materials and Ores for Cu, Zn, and Pb Recovery. *Resources* 12(3). doi: 10.3390/resources12030033.

Neuwahl, F., Cusano, G., Benavides, J.G., Holbrook, S. and Roudier, S. 2019. *Best Available Techniques (BAT) Reference Document for Waste Incineration*.

Nowak, B., Frías Rocha, S., Aschenbrenner, P., Rechberger, H. and Winter, F. 2012. Heavy metal removal from MSW fly ash by means of chlorination and thermal treatment: Influence of the chloride type. *Chemical Engineering Journal* 179, pp. 178–185.

Okada, T. and Tomikawa, H. 2013. Effects of chemical composition of fly ash on efficiency of metal separation in ash-melting of municipal solid waste. *Waste Management* 33(3), pp. 605–614.

Okamoto, B. 1990. The Fe-P (Iron-Phosphorus) System. *Bulletin of Alloy Phase Diagrams* 11, pp. 404–4012.

Tang, J., & Steenari, B. M. 2016. Leaching optimization of municipal solid waste incineration ash for resource recovery: A case study of Cu, Zn, Pb and Cd. *Waste Management*, *48*, 315–322

Tian, X., Rao, F., Li, C., Ge, W., Lara, N.O., Song, S. and Xia, L. 2021. Solidification of municipal solid waste incineration fly ash and immobilization of heavy metals using waste glass in alkaline activation system. *Chemosphere* 283.

Wang, H., Zhu, F., Liu, X., Han, M., & Zhang, R. 2021. A mini-review of heavy metal recycling technologies for municipal solid waste incineration fly ash. In *Waste Management and Research* Vol. 39, Issue 9, pp. 1135–1148.

Wen, T., Zhao, Y., Zhang, T., Xiong, B., Hu, H., Zhang, Q., & Song, S. 2020. Selective recovery of heavy metals from wastewater by mechanically activated calcium carbonate: Inspiration from nature. *Chemosphere*, *246*. Xie, K. et al. 2020. Fate of heavy metals during molten salts thermal treatment of municipal solid waste incineration fly ashes. *Waste Management* 103, pp. 334–341.

Yu, J., Sun, L., Ma, C., Qiao, Y., Xiang, J., Hu, S. and Yao, H. 2016. Mechanism on heavy metals vaporization from municipal solid waste fly ash by MgCl2·6H2O. *Waste Management* 49, pp. 124–130.

Zhang, Y., Wang, L., Chen, L., Ma, B., Zhang, Y., Ni, W. and Tsang, D.C.W. 2021. Treatment of municipal solid waste incineration fly ash: State-of-the-art technologies and future perspectives. *Journal of Hazardous Materials* 411.

Zhao, S.Z., Zhang, X.Y., Liu, B., Zhang, J.J., Shen, H.L. and Zhang, S.G. 2021. Preparation of glass–ceramics from high-chlorine MSWI fly ash by one-step process. *Rare Metals* 40(11), pp. 3316–3328.